



HAL
open science

Mud Flow Levitation on Mars: Insights from Laboratory Simulations

Petr Brož, O. Krýza, Susan J. Conway, N.T. Mueller, E. Hauber, A. Mazzini, J. Raack, M.R. R Balme, M.E. E Sylvest, M.R. R Patel

► **To cite this version:**

Petr Brož, O. Krýza, Susan J. Conway, N.T. Mueller, E. Hauber, et al.. Mud Flow Levitation on Mars: Insights from Laboratory Simulations. *Earth and Planetary Science Letters*, 2020, 545, pp.116406. 10.1016/j.epsl.2020.116406 . hal-02873081

HAL Id: hal-02873081

<https://hal.science/hal-02873081>

Submitted on 18 Jun 2020

HAL is a multi-disciplinary open access archive for the deposit and dissemination of scientific research documents, whether they are published or not. The documents may come from teaching and research institutions in France or abroad, or from public or private research centers.

L'archive ouverte pluridisciplinaire **HAL**, est destinée au dépôt et à la diffusion de documents scientifiques de niveau recherche, publiés ou non, émanant des établissements d'enseignement et de recherche français ou étrangers, des laboratoires publics ou privés.

Mud Flow Levitation on Mars: Insights from Laboratory Simulations

P. Brož^{1*}, O. Krýza¹, S. J. Conway², N. T. Mueller³, E. Hauber³, A. Mazzini⁴, J. Raack⁵, M.R. Balme⁶,
M.E. Sylvest⁶ and M. R. Patel^{6,7}

¹Institute of Geophysics of the Czech Academy of Sciences, Boční II/1401, 141 31, Prague, Czech
Republic

²CNRS UMR-6112 Laboratoire de Planétologie et Géodynamique, Université de Nantes, France

³Institute of Planetary Research, DLR, Rutherfordstr. 2, 12489, Berlin, Germany

⁴Centre for Earth Evolution and Dynamics (CEED), University of Oslo, Norway

⁵Institut für Planetologie, Westfälische Wilhelms-Universität Münster, Germany

⁶School of Physical Science, STEM, The Open University, Milton Keynes, UK Open University, Milton
Keynes, United Kingdom

⁷Space Science and Technology Department, STFC Rutherford Apple-ton Laboratory, Oxford, UK

Corresponding Author

Petr Brož

Institute of Geophysics of Czech Academy of Sciences (CAS) v.v.i

Boční II/1401

14131 Prague 4

Czech Republic

Petr.broz@ig.cas.cz

+420267103063

22 **Abstract**

23 Sediment mobilisation occurring at depth and ultimately manifesting at the surface, is a process
24 which may have operated on Mars. However, the propagation behaviour of this mixture of water and
25 sediments (hereafter simply referred to as mud) over the martian surface, remains uncertain.
26 Although most of the martian surface is below freezing today, locally warmer surface temperatures do
27 occur, and our current knowledge suggests that similar conditions prevailed in the recent past. Here, we
28 present the results of experiments performed inside a low pressure chamber to investigate mud
29 propagation over a warm (~295 K) unconsolidated sand surface under martian atmospheric pressure
30 conditions (~7 mbar). Results show that the mud boils while flowing over the warm surface. The gas
31 released during this process can displace the underlying sand particles and hence erode part of the
32 substrate. This “entrenched” flow can act as a platform for further mud propagation over the surface.
33 The escaping gas causes intermittent levitation of the mud resulting in enhanced flow rates. The mud
34 flow morphologies produced by these phenomena differ from those produced when mud flows over
35 a frozen martian surface as well as from their terrestrial counterparts. The intense boiling removes
36 the latent heat both from the mud and the subsurface, meaning that the mud flow would eventually
37 start to freeze and hence changing again the way it propagates. The diverse morphology expressed
38 by our experimental mudflows implies that caution should be exercised when interpreting flow
39 features on the surface of Mars and other celestial bodies.

40 **1. Introduction**

41 The surface of Mars is characterized by features with various shapes (Fig. 1a,b) ranging from
42 decimetres to kilometres in scale whose origin has been attributed to the action of sedimentary volcanism
43 (e.g., Allen et al., 2013; Hemmi and Miyamoto, 2018; Oehler and Allen, 2012; Pondrelli et al., 2011;
44 Salvatore and Christensen, 2015; Skinner and Mazzini, 2009; Skinner and Tanaka, 2007; Okubo, 2016;
45 Komatsu et al., 2016; Rubin et al., 2017; Brož et al., 2019, Wheatley et al., 2019; Kumar et al., 2019).
46 However, this interpretation is not unanimous, as igneous volcanism has also been proposed as a
47 formation mechanism for several of these features (e.g. Brož and Hauber, 2013; Brož et al., 2017).
48 Regardless of this ambiguity, if sedimentary volcanism (Oehler and Etiope, 2017) has ever been present

49 on Mars, the mud would propagate in an environment significantly different from the terrestrial one, in
50 particular with respect to atmospheric pressure and gravity.

51 Until recently it remained unclear as to whether such different environmental conditions would even
52 allow mud to propagate over the martian surface. This uncertainty was related to the fact that the martian
53 low-pressure environment inhibits the sustained presence of liquid water on the planet's surface (e.g.,
54 Bargery et al., 2010; Hecht, 2002). Previous studies have shown that water would boil and this could
55 significantly affect sediment transportation (Conway et al., 2011; Massé et al., 2016; Raack et al., 2017;
56 Herny et al., 2018). These results suggest that martian environmental conditions may have a profound
57 effect on mud rheology and hence its propagation may vary from our terrestrial experience.

58 On Earth, the effusion rates and volumes of ascending mud vary, and affect the sizes, thicknesses
59 and shapes of mud flows. Low effusion rates lead to the formation of flows a few centimetres-thick
60 capable of propagating up to several meters (Fig. 1c,d,e). In contrast, high effusion rates and volumes
61 may lead to flows metres thick capable of propagating over kilometres. However, the sizes and
62 thicknesses of mud flows strongly depends on its viscosity which is mainly linked to the water content.
63 Water-dominated mud flows have thicknesses varying from metres to centimetres. This is because the
64 flows preferentially spread laterally and therefore their thicknesses decreases towards the margins
65 forming overlapping lobes.

66 While the behaviour of mud during emplacement and its rheology under terrestrial conditions is
67 well studied and understood (e.g., O'Brien and Julien, 1988; Laigle and Coussot, 1997 and references
68 therein), this is not the case for Mars, nor for other planetary bodies within the Solar System, where
69 sedimentary volcanism has also been proposed (e.g., Ruesch et al., 2019). An initial study examining
70 the general behaviour of kilometre-sized mud flows in a low pressure environment was performed
71 by Wilson and Mouginis-Mark (2014), where some aspects of mud propagation over the martian
72 surface were discussed from a theoretical point of view. The authors proposed that the water present
73 in the mud would be unstable and hence evaporate from the mud flow, ultimately removing the latent
74 heat from the mixture. As a consequence, the residual water within mud should freeze in a relatively
75 short period of time, hours to days. Recent insights came from experimental work of Brož et al. (in

76 press) in which the behaviour of low viscosity mud was experimentally studied in a low pressure
77 chamber that partly simulated the environment of Mars. Their work demonstrated that low viscosity
78 mud flows can propagate over a cold (<273 K) surface under martian atmospheric pressure, however,
79 the mechanism of such propagation would be very different from that observed on Earth. On Mars, mud
80 would rapidly freeze due to evaporative cooling (Bargery et al., 2010) forming an icy-crust leading to
81 the propagation of the decimetre thick mud flows resembling pahoehoe lava flows on Earth (Brož et al.,
82 in press).

83 The average temperature of the martian surface today is far below the freezing point of water, but
84 thermal infrared observations (e.g. Sinton and Strong, 1960; Kieffer et al., 1977; Christensen et al., 2001)
85 show locally higher temperatures can occur at certain locations at favourable seasonal times (Hecht,
86 2002). This is mainly because the redistribution of solar heat is impeded by the low atmospheric
87 pressure, which limits advective heat transport by the atmosphere, and by the low thermal conductivity
88 of the regolith covering most of the surface (e.g. Presley and Christensen, 1997). Numerical thermal
89 models of the surface have been developed to derive regolith thermophysical properties such as albedo
90 and thermal inertia from the observed temperatures (e.g. Kieffer et al., 1977, Putzig and Mellon, 2007).
91 Conversely, we can use such models and the thermophysical properties to calculate the subsurface
92 temperature structure that is consistent with observed temperatures. The results are shown in Fig. 2 and
93 the details of calculations are described below in Section 2.2. Our data show that conditions above
94 freezing are not rare on Mars and that some significant amount of heat can be released to potentially
95 keep a mud flow from freezing.

96 The goal of this manuscript is therefore to investigate the behaviour of low viscosity mud flowing
97 under martian pressure conditions over a warm (from ~292 K to ~296 K) surface. More specifically, we
98 examine how the instability of water within the mud would change its flow behaviour during the phase
99 change from liquid to gaseous. Hence, we aim to reveal which transport processes would be reasonable
100 to expect during sedimentary volcanism on Mars and how they may affect the final morphology of the
101 resulting mud flows.

102 2. Methods

103 2.1. Experimental setup

104 We performed a set of experiments (see Table 1 for details) using the Mars Simulation Chamber at
105 the Open University (UK). The chamber was equipped with a 0.9×0.4 m aluminium tray filled with a
106 ~ 2 cm deep sediment bed (natural sand, $\sim 200 \mu\text{m}$) together with a reservoir containing 500 ml of low
107 viscosity, and hence water-dominated, mud ($12.7 \text{ mPa}\cdot\text{s}$ at $\sim 276 \text{ K}$ and $10.7 \text{ mPa}\cdot\text{s}$ at $\sim 296 \text{ K}$). The
108 container with the mud hung ~ 5 cm above the tray (Figure 3). Before depressurisation, the mud and sand
109 were at room temperature (from $\sim 292 \text{ K}$ to $\sim 296 \text{ K}$). The tray was inclined by 5° and 10° to force the
110 mud to move under gravity once poured onto the surface. The mud was released from the container
111 under reduced pressure (~ 7 mbar) and the movement of the mixture was observed and recorded by four
112 cameras from different angles. In some experiments the sand bed was replaced by a smooth plastic plate
113 inclined by 5° to assess if the observed processes were dependent on the presence of unconsolidated and
114 porous material. We also performed comparative experiments under terrestrial pressure to get a
115 reference set of experiments. In an additional experimental setup, a plastic box (0.6×0.4 m) filled by a
116 33 cm thick layer of sand was used to investigate the depth to which the mud is able to propagate
117 vertically. Each experiment was performed in triplicate to confirm the reproducibility of the results.

118 The mud used for the experiments was a mixture of deionised water with 0.5% w/w of dissolved
119 magnesium sulphate salts (MgSO_4) and clay at ~ 6.5 % of the mud mass (the mass ratio between
120 deionised water and clay was 4:1). The magnesium sulphate salt, which has previously been detected
121 on the martian surface (Clark, 1978; Vaniman et al., 2004; Hecht et al., 2009), was added to achieve the
122 average river water salinity which is necessary to suspend submillimetre clay particles (Corradi et al.,
123 1994). As there is no direct in-situ knowledge of which types of clays could be involved in the subsurface
124 sediment mobilisation on Mars, we decided to use the clay obtained from the claystone named after the
125 Rokle locality situated near the town Kadaň in the Czech Republic and operated by the private company
126 Keramost. This clay is a bentonite composed of 76% montmorillonite, 23% illite, and 1% kaolinite and
127 formed by alteration of pyroclastic rocks. As explosive volcanism was likely common on Mars (e.g.,
128 Wilson and Head, 1994), to a first approximation this material is a suitable analogue. The mud mixture

129 was obtained using a blender for 3 minutes to reduce the presence of more lithified clayey aggregates.
130 The average density of the resulting mixture was 1037.5 kg/m^3 . The viscosity was measured at the
131 Institute of Hydrodynamics of the Czech Academy of Science by using Haake Rotovisco RV 20 and
132 Viscotester VT 550 rheometers with ledges on the MV2 cylinder to prevent slip of the measured material
133 on its walls.

134 2.2. Modelling of Mars surface temperatures

135 To model the subsurface temperature on Mars we used the albedo and thermal inertia maps derived
136 by Putzig and Mellon (2007) from Thermal Emission Spectrometer data (Christensen et al., 2001).
137 Thermal inertia is the square root of the product of thermal conductivity, bulk density, and specific heat
138 capacity. Since the latter two exhibit much less variability in regolith than the former, we assume they
139 are constant. Density is assumed to be 1300 kg/m^3 and heat capacity is assumed to be 630 J/kg/K from
140 the numbers recommended for the InSight landing site (Morgan et al., 2018).

141 The variables governing the boundary conditions are Mars' orbit and spin axis obliquity, as well as
142 atmospheric pressure and dust optical thickness. For our modelling we use the timeseries output of the
143 local surface atmospheric pressure and local dust optical thickness at the 610 Pa pressure level provided
144 by the average climatology scenario of the Mars Climate Database (MCD, Forget et al. 1999, Millour et
145 al. 2017). The database covers the average of TES observations over martian years 24 – 31, with planet
146 encircling dust events excluded (Montabone et al., 2015). We scale the dust opacity to the local
147 atmospheric column by multiplying with the ratio of local pressure to 610 Pa (Montabone et al., 2015).
148 For the calculations of subsurface temperature, we use a 1-D version of the Mars Climate Database
149 MCD, which calculates the downwelling visible and infrared fluxes and solves the heat conduction
150 equation in the subsurface, assuming a zero heat flux lower boundary condition. The calculations are
151 done for 10×10 degree tiles, with each tile having the average surface albedo and thermal inertia, and
152 the average from the surface pressure and dust opacity timelines. The output is generated at intervals of
153 15° of solar longitude and 0.5 h of local solar time for the duration of one Mars year. The results are
154 validated by comparison with version 5.3 of the MCD and found to be consistent within a few Kelvin.
155 This dataset is searched to find the maximum surface temperatures, presented in Fig. 2a. The percentage

156 of the total time of a Mars year when the surface temperatures are above freezing is presented in Fig.
157 2b. The maximum depth of subsurface layer above freezing is shown in Fig. 2c and the maximum heat
158 that can be released from that layer before everything is below freezing in Fig. 2d.

159 **3. Observations**

160 Once the atmospheric pressure was reduced inside the chamber, the mud in the container started
161 to boil and to cool due to evaporative cooling. The boiling intensified as the pressure was decreased
162 to 12-14 mbar and continued to 7 mbar. When a pressure of ~7 mbar was reached, the mud had a
163 temperature slightly above freezing and was manually released by tipping the container, letting it
164 flow over the 'warm' (from ~292 K to ~296 K) sand surface inclined at 5°. The contact of the mud
165 with the warm surface triggered boiling, which caused ejection of sand grains to a height of several
166 centimetres. The particles landed both on the mud and on the surrounding sand. The deposition of
167 the sand grains formed a small raised rim around the contact area resulting in a crater-like depression
168 (Fig. 4, t=10 s). The explosive activity decreased with time. At the beginning, the mud was not visible
169 inside the crater area, as it was covered by a layer of loose sand grains, which was repeatedly
170 disturbed by bubbling (Fig. 4, t=10 s). Within seconds, mud could be observed on the surface – not
171 necessarily at the site where it was directly poured from the container – propagating inside the crater
172 (Fig. 4, t=22 s). At the boundary between the mud and the sand layer, a large number of millimetre-
173 scale explosion pits formed, from which gas continued to eject particles for several minutes. This
174 caused a progressive expansion of the rim.

175 Continued mud supply caused the flow to breach the sandy rim and a lobe of mud advanced over
176 the warm sand (Fig. 4, t=22 s). This flow front triggered new explosions as the mud propagated and
177 infiltrated into the surface of the sand. The escape of gas at the base of the mud flow caused the lobe
178 to vibrate vertically and to quickly levitate over the first few centimetres of the sand surface (Fig. 4,
179 t=26 s; Fig. 5a). When boiling was insufficient to lift the entire weight of the mud flow, the flow
180 lobes slid/crept over the surface entraining the sand particles. Then the lobe stalled and small
181 millimetre-scale explosions occurred around its edge forming small ridges. Simultaneously fresh
182 mud outpouring from the crater started to propagate over the lobe's surface and accumulate at the

183 front of the flow (Fig. 4, $t=30$ s). Once enough material had accumulated to overcome the small
184 ridges at the edges, a new lobe formed (Fig. 4, $t=34$ s to $t=48$ s) and the process repeated until the
185 supply of mud was exhausted (Fig. 4, $t=49$ s and $t=105$ s). The movement of mud through the lobes
186 created an interior trough with a curvy and irregular shape (Fig. 4, $t=928$ s).

187 When the same experiment was repeated with the surface inclined at 10° , a similar behaviour was
188 observed (Fig. 6). However, the flow lobes travelled faster and further than lobes at 5° inclination.
189 The resulting deposited lobes were also longer and narrower than in the previous set of experiments
190 (Fig. 6, $t=30$ s). In some cases, the flow lobe became separated from the main flow and/or from the
191 source crater by a layer of sand grains ejected by escaping gases from the sand layer (see the
192 evolution of the left flow lobe on Fig. 6 from $t=25$ s to $t=35$ s), giving the flow a discontinuous
193 appearance.

194 The boiling within the bulk volume of the mud also caused the nucleation of variously sized
195 bubbles which moved upwards to the surface of the mud. Once they reached the surface, they
196 dramatically expanded and as a result some portions of the mud were fragmented into small droplets
197 (Fig. 5b). These droplets were then ejected along ballistic pathways and deposited close to the active
198 mud flow (e.g. Fig. 4, note the presence of small dark droplets whose frequency increased around
199 the flow between times $t=30$ s and $t=105$ s). The influence of the mud fragmentation on the total
200 transported mud volume was only minor, however, it occurred over the entire length of the mud flow
201 wherever the bubbles were able to form and move through the mud. This mechanism was not active
202 during the experiments performed under terrestrial pressure conditions. Part of the ejected sand and
203 mud was also deposited on the mud flow where it formed a sandy-muddy crust (Fig. 4b) which partly
204 hindered the mud flow. The crust was either later destroyed by a new batch of mud or by a gas
205 release, or it survived until the end of the experiment.

206 We also observed the release of gases in the form of centimetre-sized bubbles for dozens of
207 minutes in the pouring area and in several other areas along the entire length of the flow providing
208 evidence that the mud remained liquid in the subsurface (Fig. 5b). The presence of liquid mud
209 covered by sand was later confirmed once the chamber was recompressed and the interior of the

210 resulting features were studied by breaking them apart from their edges to the source area (Fig. 7).
211 By using an additional experimental setup, a plastic box infilled by a 33 cm thick layer of sand, we
212 found that the mud flow was capable of eroding into the sand layer to a depth of several centimetres
213 as mud was observed beneath the original sand surface. This setup also revealed that the mud flow
214 was surrounded by a layer of sand saturated by water (Figs. 7b-d).

215 The inspection of the final morphology of the mud flows once the chamber was recompressed
216 revealed that the internal structures of the flows were supported by a hardened mixture of mud and
217 sand allowing the formation of vertical cliffs or overhangs forming crusts which fully or partially
218 covered the flow channels. These crusts enclosed cavities through which the flows had propagated
219 (Fig. 7f). We also observed that the bottoms of the troughs were covered by fine-grained clay.
220 Repeated gas explosions had formed holes which were located above small subsurface pockets
221 infilled by mud.

222 The experiments performed under terrestrial pressure did not show the same behaviour or
223 morphologies as those at martian pressure (Fig. 8). The mud within the container before pouring did
224 not boil and its internal temperature did not drop. Once the mud was poured from the container (Fig.
225 8, $t=5$ s), it started to flow relatively uniformly over the sand surface (Fig. 7f) and, as a consequence,
226 a broad and thin mud flow formed (Fig. 8, $t=20$ s). In some cases, centimetre-sized flow lobes formed
227 on the edge of the propagating flow (Fig. 8, $t=25$ s and $t=85$ s) as a result of topographic irregularities
228 in the sand layer. The flow did not significantly erode into the sand surface and vertical cliffs or
229 protective muddy-sandy crust were not observed to form.

230 The experiments performed under reduced atmospheric pressure over the 5° inclined plastic plate
231 showed that boiling still occurred, but it was not able to lift the propagating mud flow. Once the mud
232 was poured from the container, it started to flow over the surface forming a several centimetres wide
233 and a dozens of centimetres long flow. As no unconsolidated material was available, the flow did
234 not erode to the subsurface and hence the direction of the propagation of the mud flow was only
235 controlled by gravity. Analogue experiments performed under terrestrial pressure lead to the
236 formation of similarly looking mud flows, however, no boiling was observed.

237 4. Discussion

238 4.1. Application to Mars

239 Our experiments revealed that a low pressure environment has a significant effect on the
240 propagation of low viscosity mud over a warm unconsolidated surface (Fig. 9). The reason for this
241 different behaviour is the instability of water (Bargery et al., 2010) that leads to boiling and the
242 formation of water vapour bubbles which escape violently from the mud to the surrounding
243 atmosphere and partly also into the subsurface. The strongest influence of the boiling on the mud
244 movement occurs at the contact between the mud and the warm material over which the mud
245 propagates. Here the boiling is most intense as the heat stored within the substrate is available to
246 support boiling. As a result, a large quantity of water vapour is produced at this interface (Fig. 5a).
247 The release of water vapour can then modify the way the mud moves leading to levitation and
248 sliding/creeping of the advancing mud lobes.

249 This is similar to the transport mechanism described by Raack et al. (2017) and Herny et al.
250 (2018), who studied the downslope movement of water-saturated sediments in a low pressure
251 environment, albeit with one major difference. Whereas Raack et al. (2017) and Herny et al. (2018)
252 observed that the water-saturated sediments propagated in the form of individual small pellets, the
253 levitating mud observed herein moves as a coherent fluid (Figs. 2, 3 and 6a). The entire flow lobe is
254 therefore affected by the levitation. Once the gas production in the advancing lobe decreases, the
255 mud seems to propagate over the inclined unconsolidated surface by sliding and/or creeping (Figs. 2,
256 3 and 6a) as the gas release can only partly lift the lobe. These mechanisms cause an increase in the
257 speed of mud propagation over the unconsolidated surface under martian ambient pressure (Figs. 2
258 and 3) as compared to terrestrial ambient pressure (Fig. 8).

259 The boiling of water has also another effect on mud flow propagation in regard to its stability in
260 the martian environment. This is because the ejection of sandy grains by expanding gas and their re-
261 deposition on top of the mud flow can form a sandy-muddy crust by coalescing sand and finer-
262 grained clay particles together. The crust can partly isolate the liquid mud from the atmosphere and
263 prolongs its lifetime on the surface. The mud can then propagate under the crust giving rise to the

264 formation of an interconnected network of mud channels beneath the crust (e.g. experiment #26 and
265 #31).

266 The crust which developed in our experiments extended along the flow over several centimetres
267 of the mud flow channel (e.g., Figs. 4, 5, 6 and 7), but real mudflows are likely to be longer and
268 wider, so it is difficult to estimate the efficacy of this process at field-scale. We hypothesize that the
269 limited coverage of the flow in our experiments was caused by the fact that these experiments were
270 volume-limited and the processes associated with the development of the mud flow operated for only
271 a relatively short period of time. If the mud volume were larger, the flow would last for longer and
272 more mud-sand interaction would occur and perhaps a crust may be formed over a larger surface
273 area of the mud channel. If a larger section of the channel were covered by the crust, this may fully
274 isolate the flow from the low atmospheric pressure, causing boiling to cease. Under such scenario,
275 boiling would only occur at the active edges of the mud flow where the mud would be exposed to
276 the atmosphere. Even if the crust could only cover part of the channel over its entire length, our
277 observations suggest that mud propagating over a warm surface – similarly to the mud propagating
278 over a cold surface (Brož et al., in press) – is capable of developing a protective crust prolonging the
279 lifetime of the flow on the surface of Mars. This is an aspect of mud propagation that has not
280 previously considered and should be investigated further. However, it should be noted that this
281 process may only be important for martian mud flows whose width is within the range of centimetres
282 to decimetres, and less significant for wider ones. This is because even under the reduced martian
283 gravity the ballistic trajectory of the particles is limited. Furthermore, a larger width of the flow
284 would mean that the volume of ballistically transported particles, necessary to form a sufficiently
285 thick crust, would significantly increase. As a consequence it would be difficult to form a crust over
286 a flow more than several tens of centimetres wide. Therefore, decimetre-wide flows would show
287 variations on their surfaces as the flow edges (unlike the central part) would be affected by the
288 presence of a newly formed crust. Hence, the central part would display patterns associated with
289 flow processes. It should be highlighted that we predict crust formation only on martian mud flows
290 propagating over mobile substrates, such as, unconsolidated sandy regolith. As shown by the
291 experiment setup using the plastic plate, if the mud propagated over impermeable rocky or crusty

292 surfaces, even though boiling would still occur, the crust would not be formed because of the absence
293 of small particles that could be ejected onto the mud. The properties of the substrate could
294 significantly influence the way the mud propagates, and the final morphology observed at the surface.

295 We also observed that mixing of the mud and sand at the flow boundaries produced vertical cliffs
296 or even overhangs which were relatively stable as shown by their capacity to survive the processes
297 of chamber repressurisation (Figs. 7a,d and 8). We expect that within the range of centimetres to
298 decimetres wide mud flows such cliffs may result in atypical morphologies compared to those found
299 in terrestrial mud flows suggesting that comparison to terrestrial analogues could be misleading.
300 However, we do not expect that shapes of metre- or kilometre-sized mud flows would be affected as
301 the mechanical strength of such cliffs would be limited. Centimetre-sized cliffs can be attained,
302 whereas metre-sized cliffs would collapse. Small mud flows can therefore share some similarities
303 with terrestrial low viscosity lava flows for which vertical cliffs or overhangs are common (e.g.,
304 Kilburn, 2000) as lava solidification is capable of forming such landforms.

305 4.2. Temperature drop within the mud and substrate

306 In addition, our experiments show that there is another crucial factor which deserves further
307 investigation when studying surface expressions of possible martian mud flows. The instability of
308 the water causes a temperature drop in the mud due to evaporative cooling which removes latent heat
309 from the mud and from the subsurface (Bargery et al., 2010; Brož et al., in press). So, once the
310 ascending mud reaches the martian surface, the mixture would rapidly self-cool close to the freezing
311 point.

312 Specifically, when the mud initially propagates over a warm surface, and the flow continues over
313 the same area for a certain amount of time, evaporative cooling removes the available heat both from
314 the mud and the substrate. This results in gradual freezing of the mud and the subsequent formation
315 of an icy-muddy crust (Brož et al., in press), altering the mechanisms of mud propagation. Ultimately
316 the mud would propagate via frozen mud tubes in similar fashion as pahoehoe lava (Brož et al., in
317 press). This leads us to conclude that mud movement over today's martian surface would involve a
318 combined process governed both by levitation and/or sliding at the front and by freezing as the flow

319 progresses. Both mechanisms may occur during the formation of a single mud flow and this suggests
320 that the resulting morphologies may record these variations of mud transport.

321 To obtain a first order of understanding regarding what happens in case of a mud flow over a warm
322 surface, we use the subsurface temperature profiles corresponding to the maximum ground temperature
323 case in Fig. 2a as the initial temperature state. We force the top of that temperature profile to be at 273 K,
324 representing the coldest possible temperature in contact with boiling water. We then solve the heat
325 conduction equation starting from the above described condition, using the explicit Euler finite
326 difference method with 1 mm depth resolution and 0.1 s time resolution. The model is stopped when the
327 entire profile is below 273 K, the time until at that moment is presented in Fig. 2e. For comparison we
328 also conduct this cooling model with a profile resembling the laboratory setup: i.e. assuming a thermal
329 conductivity of $0.04 \text{ Wm}^{-1}\text{K}^{-1}$ for the 0.2 mm particle diameter sand at 700 Pa (Presley and Christensen,
330 1997) and an initial constant temperature of 273 K. The timescale of cooling below freezing everywhere
331 is not meaningful in this context, but we can calculate the heat flow conducted through the surface as a
332 function of time. This heat flow q with unit Wm^{-2} can be translated into a vapour column production
333 rate v with unit of m s^{-1} , which is the thickness of the vapour layer produced per second:

$$334 \quad v = q R T / (L_v m_{H_2O} P)$$

335 where $R = 8.314 \text{ J K}^{-1} \text{ mol}^{-1}$ is the ideal gas constant, $T = 273 \text{ K}$ is the assumed gas temperature, $L_v =$
336 $2.46 \times 10^6 \text{ Jkg}^{-1}$ is the latent heat of water vaporization, $m_{H_2O} = 0.018 \text{ kg}$ is the weight of 1 mol of water,
337 and $P = 611 \text{ Pa}$ is the saturation pressure of water at temperature T . Temperature and pressure below a
338 levitating flow will likely be higher, and the volume lower, than these assumed values, since it must
339 compensate for hydrostatic and ambient pressure. It is likely that for levitation a critical production rate,
340 proportional to the heat flow out of the top of the substrate must be sustained. In the laboratory
341 experiments the levitating is intermittent, with a typical duration on the order of 10 s after the
342 emplacement of fresh mud flow lobes (Fig. 4). In the thermal model of the laboratory setup with the top
343 of the substrate forced to 273 K, the heat flow conducted from the surface is $> 550 \text{ Wm}^{-2}$ in the first 10
344 seconds. This corresponds to column of vapour produced per second of $v = 46 \text{ cm s}^{-1}$. It should be noted

345 that not all of the heat from the subsurface will produce water vapour from the mud flow, some heat will
346 be transported away by the vapour.

347 Nevertheless, taking 550 Wm^{-2} as requirement for mud levitation, we can apply it to the model of
348 the forced cooling of Mars surface to estimate how long flows could levitate on Mars, Fig. 2f shows the
349 duration of heat flow $> 550 \text{ Wm}^{-2}$ conducted through the substrate surface forced to a temperature of
350 273 K starting from the maximum modelled temperature conditions (Fig. 2a). This map shows that over
351 a band of latitudes of 60°S to the equator, levitation is possible if a mud flow occurs close to noon during
352 the warmest season. In the northern hemisphere this also applies to parts of Syrtis Major Planum and
353 Chryse Planitia, due to their relatively high albedo.

354 This model neglects the observed ejection of substrate particles from below the flow, which would
355 initially increase the heat flow from the subsurface by exposing deeper layers. At some point however
356 the erosion of the substrate would expose layers below zero, so that this process would stop at most at a
357 few centimetres of depth (Fig. 2c). Also neglected is the possibility of water penetrating into the
358 subsurface, either in vapour or in liquid form, which would likely speed up cooling of the substrate.

359 We are also aware that the environmental properties on Mars vary over time, due to the chaotic
360 variation in Mars' orbital parameters, which affects the distribution of incoming insolation (Laskar et
361 al., 2004). For example, during periods of higher obliquity (Ward, 1973) areas where surface
362 temperatures could be above the freezing point of water would vary in magnitude and position. Also,
363 the depth to which the freezing point would descend would vary (Costard et al., 2002) and hence the
364 amount of available heat necessary to keep the process of the violent boiling active would be
365 different. The time required by the evaporative cooling to remove the available heat from the
366 subsurface increases proportionally with the depth of the freezing point. Variations in surface
367 temperatures caused by variations in Mars' orbital parameters may therefore prolong or foreshorten
368 the period over which boiling would dominate the behaviour of the mud. This means that the
369 mechanisms dominating in mud propagation should change through time.

370 Additionally, the complex magmatic history of Mars (e.g. Grott et al., 2013) suggests that the heat
371 flux within the martian crust has not been steady. In fact, it has varied through time at various

372 localities producing geothermal anomalies (e.g. Plesa et al., 2016). These sites may represent ideal
373 places where sedimentary eruptions may result due to the melting of subsurface water ice or
374 hydrothermal activity. Higher heat flux may also imply that the surface can be sufficiently warm to
375 prevent the freezing of the extruded mud for extended periods of time, or even completely inhibited.
376 Under such a scenario, it may be possible that the described processes, which operated in our
377 experiments at the centimetre-scale only, would be able to affect even wider surfaces and therefore
378 produce larger scale mud features. It should therefore be taken into account that some morphologies
379 which are present at the surface of Mars today, and which may have an origin associated with mud
380 eruptions, may be linked to the intense boiling and the above described transport mechanisms.

381 4.3. Scaling to Mars and experimental limitations

382 The presented experimental approach has several limitations as it cannot fully attempt to simulate
383 all the conditions of sedimentary volcanism on Mars or even on Earth. Firstly, our experiments were
384 performed with a fixed volume of mud (500 ml). This limits the size of the resulting flows to a length
385 of several decimetres, the width to several centimetres and the thickness to less than 1-2 centimetres.
386 On Earth, sedimentary volcanism can extrude mud volumes several orders of magnitudes larger than
387 those in our experiments (e.g. Kopf, 2002; Mazzini and Etiope, 2017) resulting in metre- to
388 kilometre-long mud flows. However, low volume eruptions are more common than voluminous ones.
389 Obviously, we were not able to perform experiments at the metre- to kilometre-scale due to the size
390 limitation of the available low pressure chamber. Nevertheless, our work can still provide valuable
391 insights into mud propagation in a low pressure environment due to the chosen mud viscosity. This
392 is because low viscosity mud flows, naturally occurring on Earth, propagate over flat surfaces
393 preferentially on their edges forming centimetres-thick mud lobes (Mazzini and Etiope, 2017; Miller
394 and Mazzini, 2018) similar to those observed in our experimental setup. Therefore, we are capable
395 to directly address, some of the differences between those terrestrial flows and putative martian
396 analogues. Our work therefore suggests that environmental differences between Earth and Mars
397 would affect the propagation of both small and large martian mud flows, but with differing intensity.
398 However, our experiments do not provide appropriate insights about the propagation of thicker low
399 viscosity flows, for example, when the mud becomes channelized or a large quantity of mud is

400 extruded over a short period of time. This is because in thick mud flows the flow regime may change.
401 This should significantly change the way the mud propagates in the low pressure environment as
402 heat will be transported differently within the flow and there is a need for further experimental or
403 theoretical investigation of this problem.

404 An additional limitation is associated with the inability to perform experiments in a reduced gravity
405 environment, mimicking the gravity of Mars (3.7 m s^{-2}). Our experiments were performed under
406 terrestrial gravity (9.8 m s^{-2}), which has an influence on the way the mud propagates. Terrestrial gravity
407 limited the height to which the vibrating mud could levitate as well as the total volume of mud which
408 could be lifted. A similar limitation was encountered in the study of Raack et al. (2017) in which the
409 different gravitational force affects the levitation of the sedimentary pellets propagating over the hot
410 surface. These authors showed that the reduced gravity would allow pellets to levitate for up to 48 times
411 longer on Mars than on Earth and that the lifted pellets could be up to seven times heavier compared to
412 those lifted in their experiments. These calculations suggest that, on Mars, mud would levitate for a
413 longer period of time and to a greater height than observed in our experiments. The lower martian gravity
414 would also affect the distance to which the sand grains and small mud droplets would be ejected. Brož
415 et al. (2014) showed that ballistically emplaced scoria particles can travel about 20 times further on Mars
416 than on Earth due to the lower gravity and lower atmospheric pressure. Therefore, the ejected material
417 would be spread over much wider area than observed in our experiments. This means that on Mars more
418 transported material would be necessary to build a steep-sided rim which in part affects the flow of
419 material over the flat surface. As a consequence, the role of marginal rims to, at least partly, guide the
420 flow direction may be limited on Mars as the rims may be much broader but shallower than those
421 observed in our experiments. Ultimately gravity may also affect the way the flow erodes the subsurface
422 as sand and other particles would be more easily shifted by the gases released from the advancing mud
423 flow. To overcome these limitations, it would be necessary to develop a dedicated numerical model and
424 perform additional analogue experiments which would allow better understanding of the behaviour and
425 rheology of mud under reduced atmospheric pressure. This approach would allow direct comparison of
426 modelled features with real martian landforms. This goal is beyond the scope of our present work.

427 **5. Conclusions**

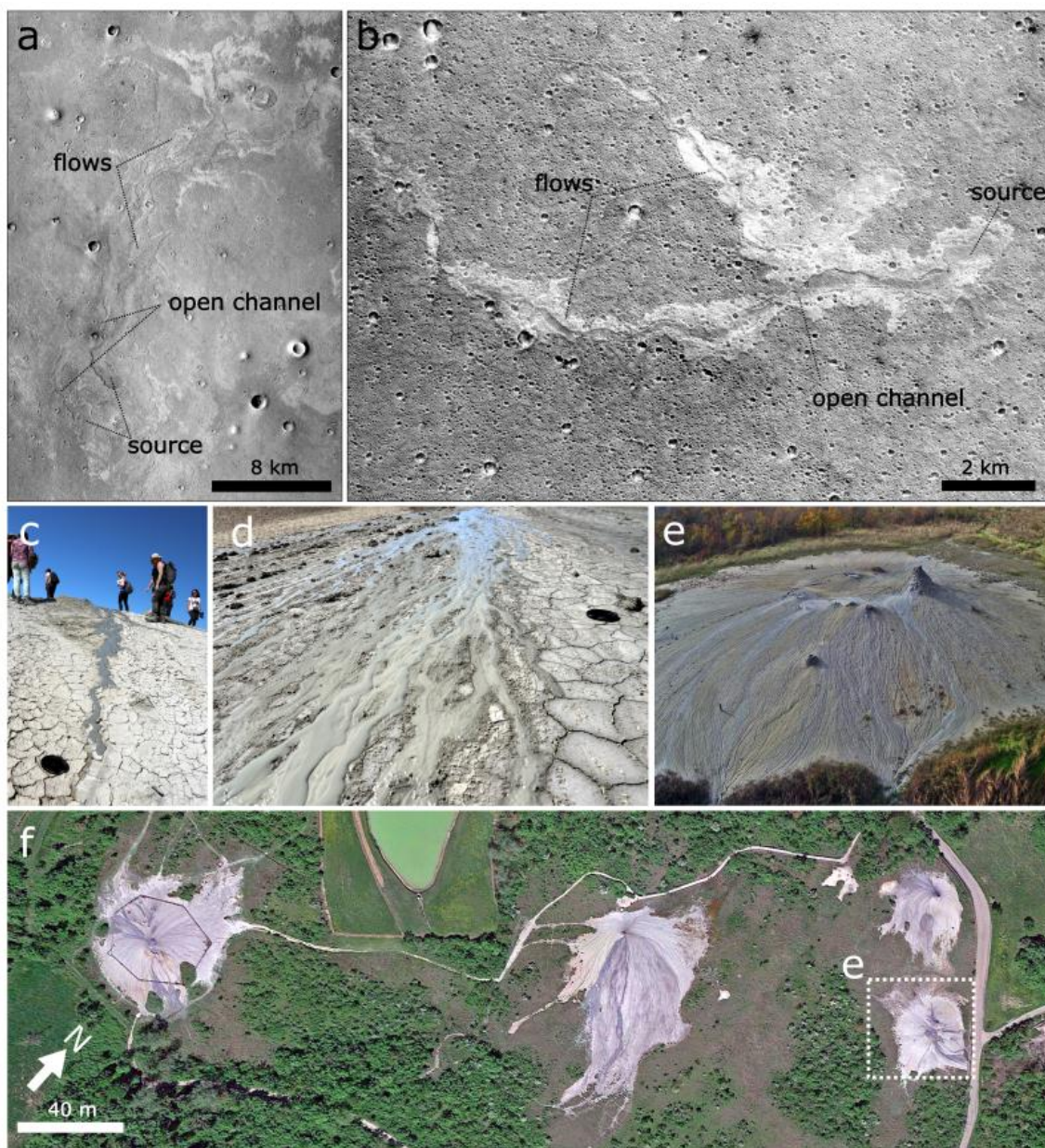
428 Our experiments show that a warm (from ~292 K to ~296 K) and unconsolidated surface has a
429 profound effect on the behaviour of flowing low viscosity mud in a low-pressure environment (Fig.
430 9). The resulting boiling occurring during the mass flow, causes transient levitation of the mud above
431 the warm surface as well as the erosion of the unconsolidated sandy substrate. Both mechanisms alter
432 mud propagation in a low pressure environment. Moreover, we expect that these processes would be
433 even more effective on Mars which has a lower gravitational acceleration than on Earth. On Mars
434 gravity does not change the boiling rate, but the sediments can be more easily entrained (Raack et
435 al., 2017; Hery et al., 2018). The gas release should levitate mud for a longer period of time than
436 observed in our experiments, as also similarly suggested for wet sand (Raack et al., 2017; Hery et
437 al., 2018), hence allowing the mud to propagate over larger distances than modelled within the low
438 pressure chamber. Additionally, as the process of evaporative cooling would remove the latent heat
439 from the mud and from the surface over which it is propagating, at a certain point, the mud would
440 start to freeze. This would cause the formation of a protective icy-muddy crust affecting the way the
441 mud moves (Brož et al., in press) switching from levitation and sliding/creeping to the propagation
442 via mud tubes. The mechanisms of mud propagation on Earth at different pressure-temperature
443 conditions are well studied. Mud propagation, during this relatively simple process, is controlled by
444 mass gravity flow. In contrast, very little is known about the modes controlling the same events on
445 Mars and other bodies with or without atmospheres where mud eruptions may be present (e.g.,
446 Ruesch et al., 2019). Our new data demonstrate that the behaviour of mud and its propagation in a
447 low-pressure environment, is strongly controlled by the surface temperature since freezing or rapid
448 boiling give rise to different transport mechanisms than simple liquid flow. We conclude that mud
449 eruption activity on other celestial bodies may produce profoundly different morphologies compared
450 to those commonly observed on Earth.

451 **Acknowledgements**

452 The access to the Large Mars Chamber at the Open University was provided by Europlanet 2020 RI
453 which has received funding from the European Union's Horizon 2020 research and innovation program

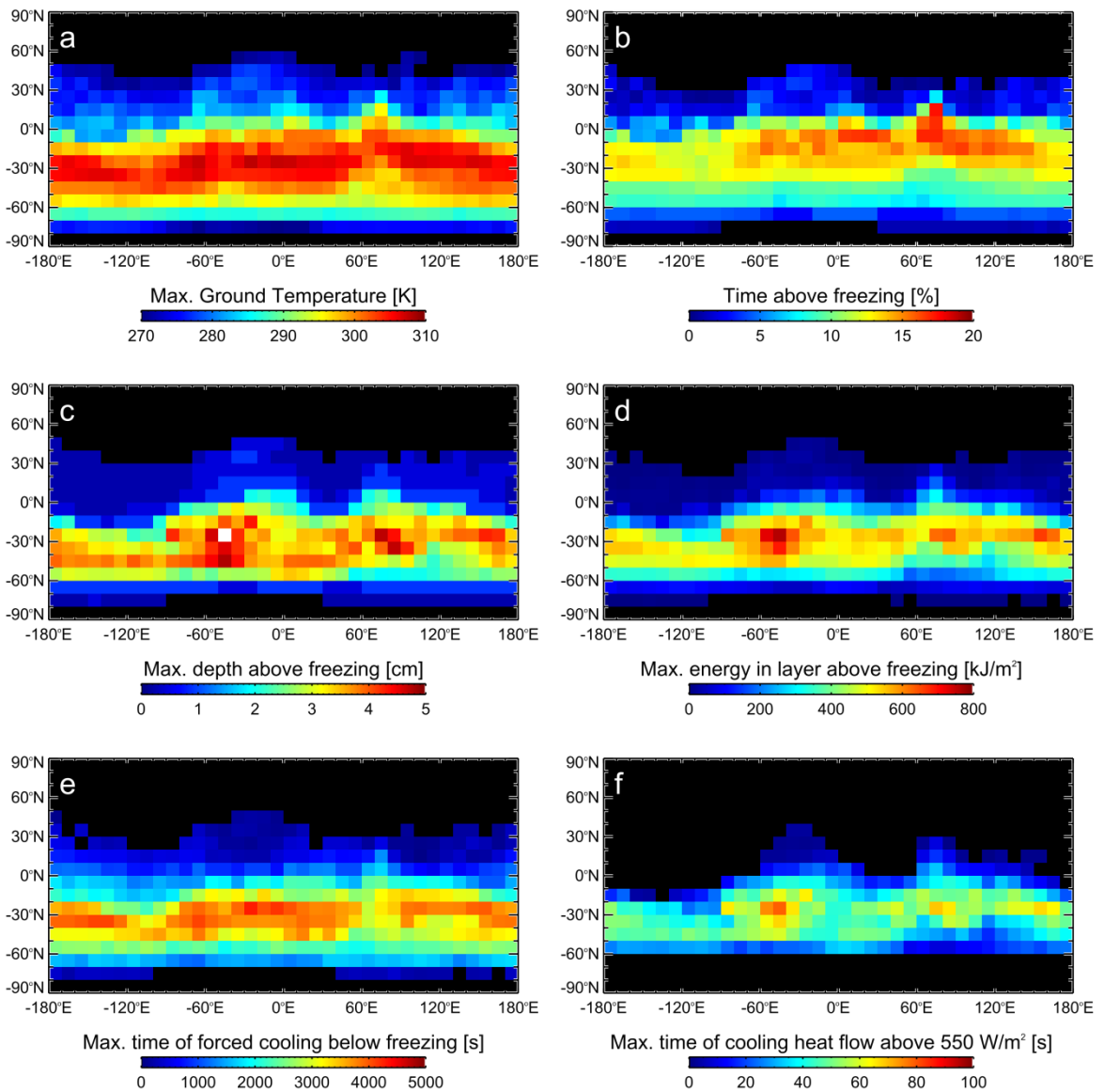
454 under grant agreement No 654208. OK was supported by Center for Geosphere Dynamics (Faculty of
455 Science at Charles University) project UNCE/SCI/006. AM was funded by the ERC grant agreement
456 308126 (LUSI LAB) and the Research Council of Norway (Centers of Excellence funding scheme,
457 project 223272). We are thankful to Mikhail A. Ivanov and two anonymous reviewers for their
458 constructive comments and to William McKinnon for handling the editorial process. The movies and
459 temperature and pressure data that support the findings of this study are available in Zenodo.org with
460 the identifier 3520947 (<https://doi.org/10.5281/zenodo.3520947>).

461 **6. Figures and tables**



462

463 Figure 1. Examples of putative martian low viscosity mud flows and their meter-sized terrestrial
464 counterparts. Panels a) and b) show two examples of putative kilometre-scaled martian water-dominated
465 mud flows within the Chryse Planitia (Komatsu et al., 2016, Brož et al., 2019). c) and d) show meter-
466 sized low viscosity mud flows within the crater of Bakhar mud volcano in Azerbaijan which, during
467 prolonged activity, are capable of building dozens of meter-sized morphological features. e) shows
468 mud volcanos within the area of Salse di Nirano in Italy and f) shows the scale and context of this feature
469 where other similar features are present. Panel a) (centred at 19.16°N, 322.73°E) and panel b) (centred
470 at 20.24°N, 324.01°E) are based on CTX images F05_037598_1988_XN_18N037W and
471 B19_016856_1990_XI_19N035W respectively, image credit NASA/JPL/MSSS. Panel f) based on
472 Google Earth™.



473

474

Figure 2. Results of thermal model calculations described in the Section 2.2. Panel a) is the map of the

475

maximum temperature the surface can be expected to attain in an average current martian climate. b) is

476

the total percentage of a Mars Year that the surface is above 273.16 K. c) shows the maximum depth of

477

the layer that experiences temperatures above 273.16 K. d) shows the maximum energy that can be

478

released before the entire surface layer is cooled below 273.16 K. e) shows the time needed to cool the

479

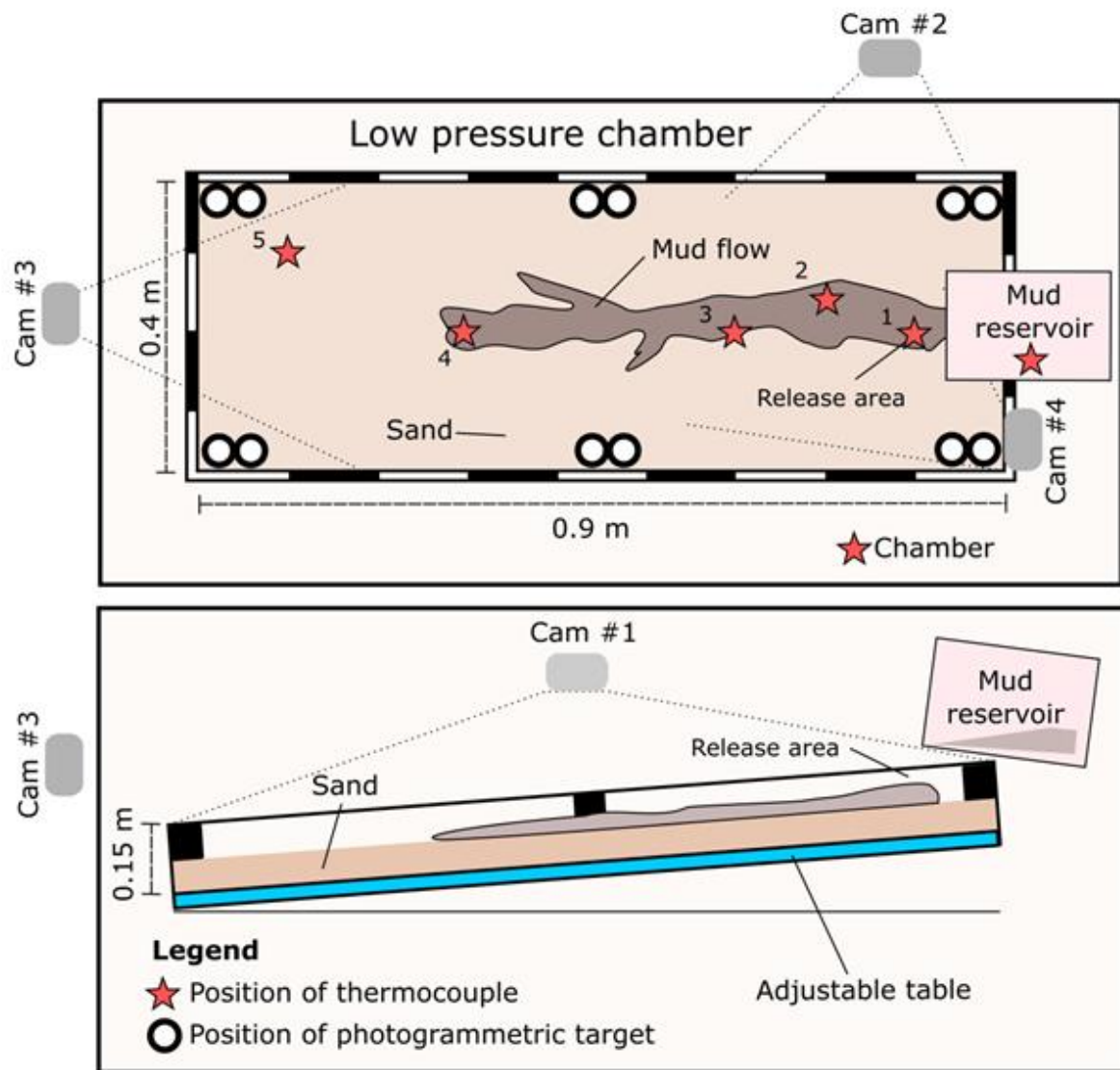
subsurface from the maximum temperature case (a) to below 273.16 K when the substrate top is forced

480

to be at 273.16 K. f) shows the time needed until the heat flow conducted through the surface drops

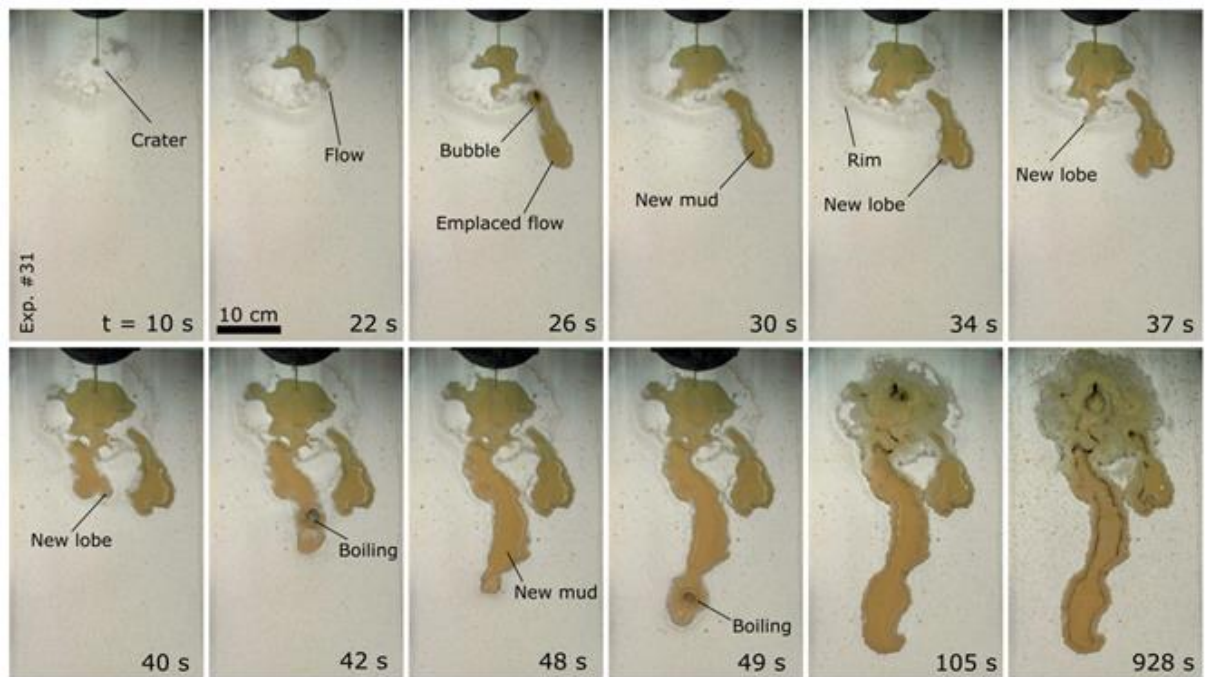
481

below 550 W/m² under the same conditions as in e).



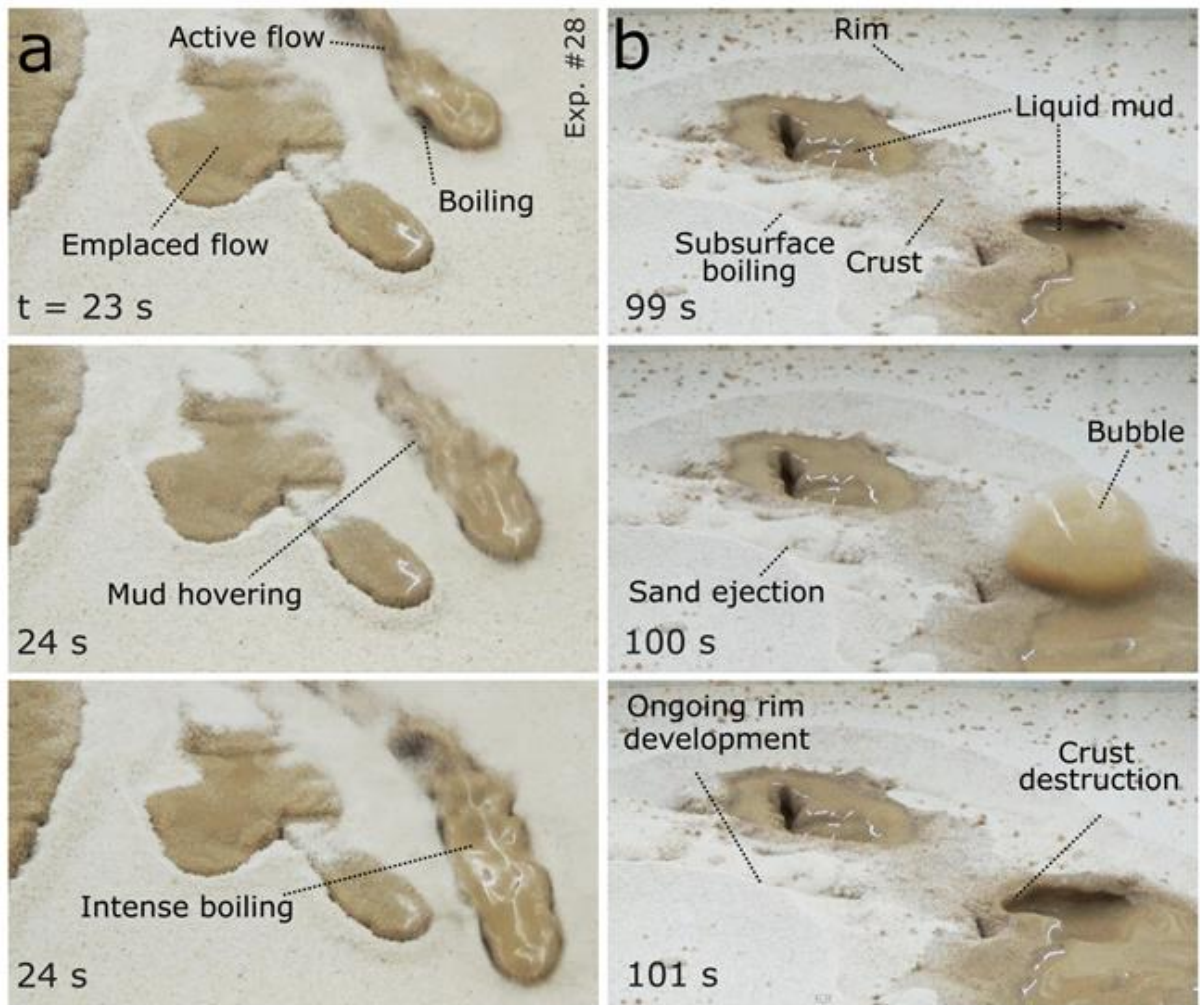
482

483 Figure 3: Schematic illustration showing the experimental setup with the position of thermocouples,
 484 photogrammetric targets and four cameras marked. Data from thermocouples are not discussed within
 485 this study, however, they are provided in the Supplementary materials uploaded on Zenodo.org for those
 486 who are interested.



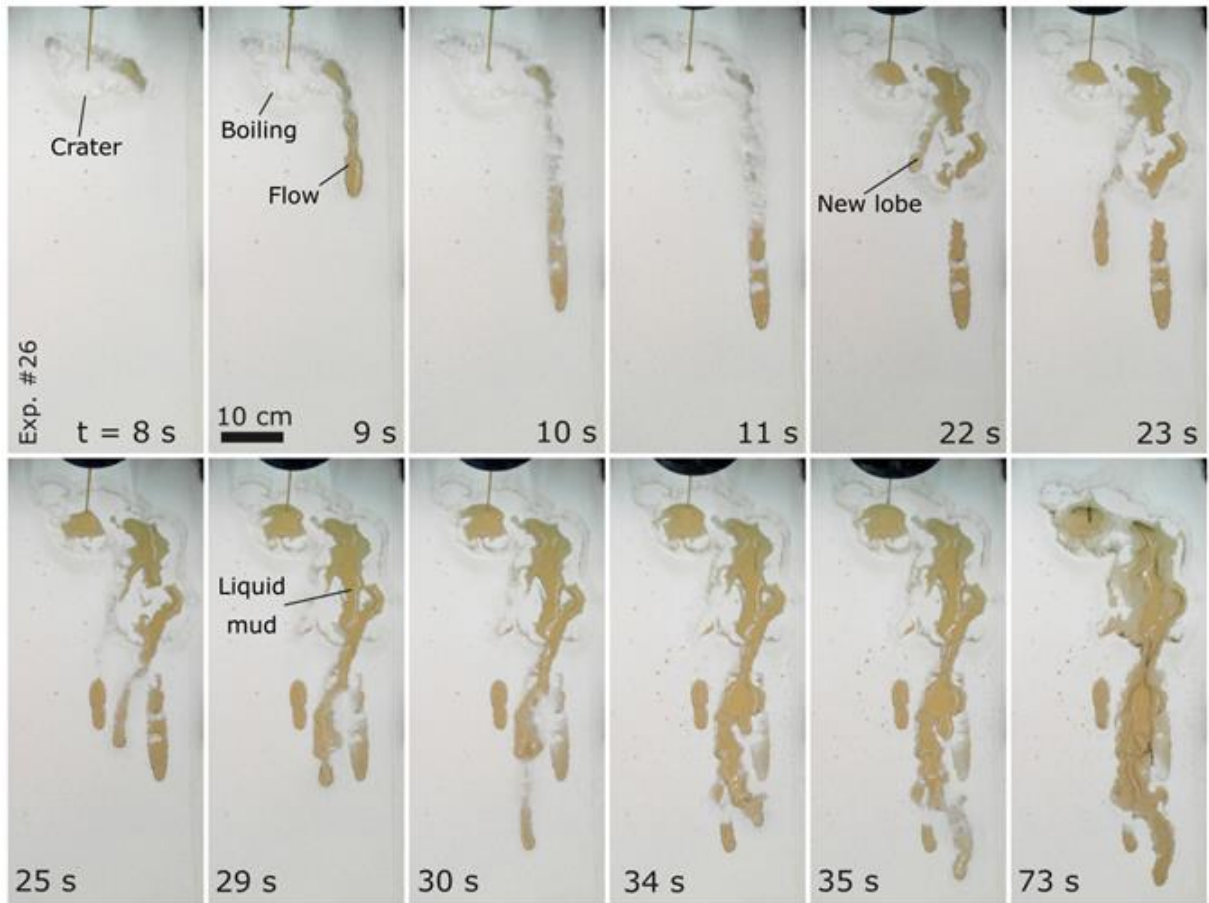
487

488 Figure 4: A sequence of images from different time steps (in seconds) capturing the propagation of
 489 low viscosity mud over a warm surface inclined by 5° under low pressure mimicking conditions on
 490 Mars. The mud was poured on the surface from a hanging container. Once the mud touched the surface,
 491 intense boiling occurred, and a central crater-like depression started to form (t=10 s). Soon a surface
 492 mud flow developed (t=22 s) and started to propagate downslope a few centimetres at a time in the form
 493 of a narrow lobe which was levitating and sliding/creeping over the sand surface (t=26 s). After a while,
 494 the flow stopped its propagation (t=30 s) and a new lobe developed (t=34 s). This process repeated as
 495 long as mud was being poured onto the surface (t=37 s; t=40 s). The boiling also caused the formation
 496 of rims surrounding the lobes. The images were obtained from the video recorded by camera #1
 497 observing experiment #31 from above.



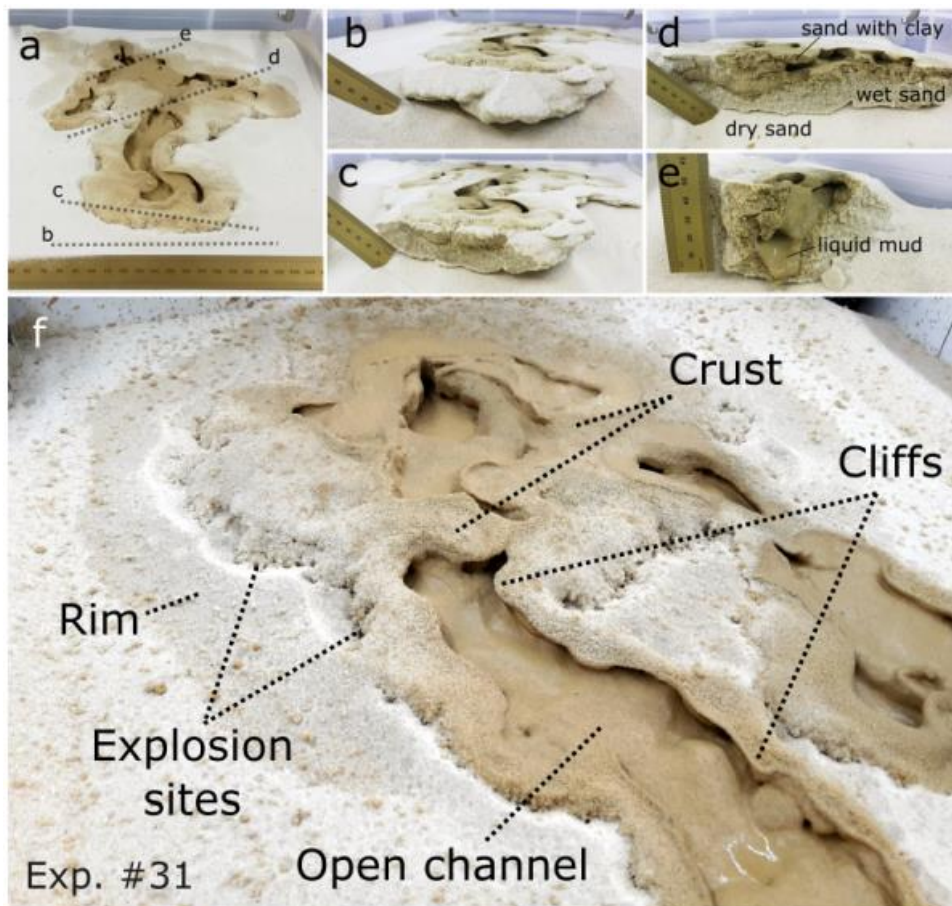
498

499 Figure 5: Two-time sequences of images showing (a) the levitating and sliding mud over an
 500 unconsolidated surface and (b) the continuous explosions indicating the presence of liquid mud in the
 501 subsurface. Note the irregular shape of the propagating active mud flow in the vertical direction in panel
 502 (a) revealing intense boiling within the flow and associated release of water vapour from the flow. Such
 503 releases caused levitation of the material and rapid propagation of the flow over the surface. The images
 504 were obtained from the video recorded by camera #3 observing experiment #28 from front.



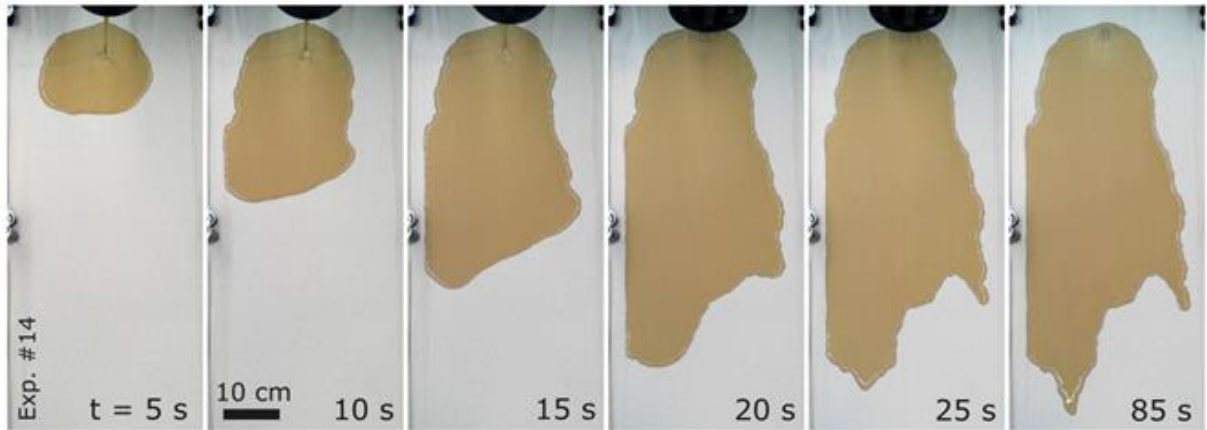
505

506 Figure 6: A time series of images (time steps in seconds) capturing the propagation of low viscosity
 507 mud over a warm surface inclined by 10° under low pressure, mimicking conditions on Mars. The mud
 508 was poured to the surface from a hanging container. Similarly to the results captured in Figure 3, intense
 509 boiling occurred ($t=8$ s) and after a while a narrow mud lobe developed ($t=9$ s). Due to the higher
 510 inclination of the surface the mud lobe travelled faster and further ($t=11$ s) than in those experiments
 511 performed at a slope of 5° . The narrow, long lobes were partly or fully covered by ejecting sandy grains
 512 ($t=25$ s) which caused a seemingly discontinuous appearance of the final morphology. The images were
 513 obtained from the video recorded by camera #1 observing experiment #26 from above.



514

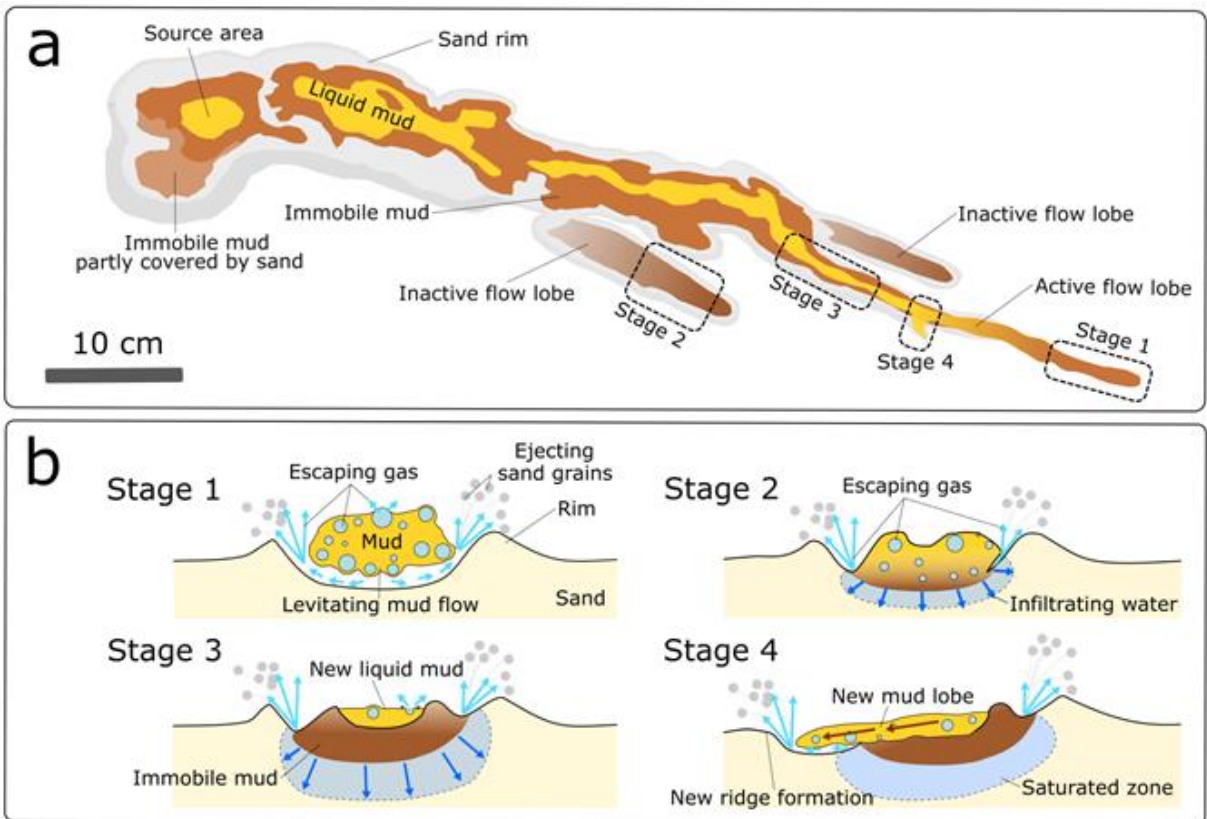
515 Figure 7: An example of the resulting morphology of a low viscosity mud flow and its inner structure
 516 formed by the movement over “warm” sand in a low pressure environment. (a) The edge of the flow is
 517 surrounded by set of sandy ridges and several central troughs through which the mud propagated. The
 518 dashed line at b marks the position at which the mud flow was exposed by removing the sand (shown in
 519 panel b) and the dashed lines c to e mark where the flow was sectioned to reveal the inner structure of
 520 the flow (shown in the corresponding panels). The flow was composed of a layer in which clay-particles
 521 dominated and by a layer in which the sand was saturated by water (marked on panel d). In some cases,
 522 the liquid mud was still present in the subsurface (e). f) Detail of the resulting low viscosity mud flow
 523 morphology, which was characterised by a network of open central channels of varying depths
 524 surrounded by rims composed of sandy particles ejected from multiple small explosion sites. These
 525 explosion sites mark the boundary between the liquid mud and surrounding dry sand. In some places a
 526 protective crust developed by gluing together clay and sand particles. The width of the main channel is
 527 around 2 cm. Note the cliffs which can be vertical or overhangs can be formed.



528

529 Figure 8: A sequence of images taken at different time steps (t) capturing the propagation of low
 530 viscosity mud over a warm surface inclined by 5° under terrestrial ambient pressure conditions. The
 531 mud propagates as a tens of centimetres wide and a few mm thick sheet-like mud flow. Images obtained
 532 from the clip recorded by camera #1 observing the experiment #14 from above.

533



534

535 Figure 9: Schematic illustration showing the development of a low viscosity mud flow during the
 536 movement over the 'warm' inclined surface under martian conditions with insets showing the main

537 processes operating during its emplacement. (a) The ascending mud would move downhill from the
538 source area via partly overlapping flow lobes. The instability of water within the mud would cause
539 redeposition of unconsolidated sandy surface as well as fast propagation of the fronts of the active lobes.
540 The different colours mark different states of the mud; brown indicates immobile mud, while orange
541 indicates liquid, and hence mobile, mud. The black dashed rectangles mark the position of small insets
542 in panel **b** (b) **Stage 1** shows mud propagation by levitation over the inclined sand surface. The levitation
543 is caused by boiling water releasing gases from the base of the mixture. Escaping gases are additionally
544 able to trigger ejections of sand grains and hence cause self-burying of the mud flow under the surface.
545 **Stage 2** shows the situation when the mud flow lobe stops propagating by levitation and when the water
546 from the mud starts to infiltrate into the subsurface. **Stage 3** then shows the input of new liquid mud
547 flows over the older mud flow. Finally, at **Stage 4** the new batch of mud overcomes the margins of the
548 older mud flow and hence the mud flow would be again be exposed to a warm surface. This then causes
549 the levitation of the mud flow and repetition of the whole process.

Exp #	Pressure range* [mbar]	Inclination [°]	Release time** [s]	Type of surface
exp_31	7.1-8.1	5	52	~2 cm sand layer
exp_32	6.9-7.6	5	29	~2 cm sand layer
exp_33	6.9-7.4	5	21	~2 cm sand layer
exp_51	7.0-7.7	5	45	~33 cm sand layer
exp_52	6.6-7.1	5	34	~33 cm sand layer
exp_53	6.6-8.5	5	22	~33 cm sand layer
exp_12	1000	5	19	~2 cm sand layer
exp_13	1000	5	20	~2 cm sand layer
exp_14	1000	5	18	~2 cm sand layer
exp_26	6.7-7.4	10	36	~2 cm sand layer
exp_27	7.1-8.1	10	23	~2 cm sand layer
exp_28	7.1-7.8	10	43	~2 cm sand layer
exp_46	6.7-7.6	5	34	plastic plate
exp_47	6.9-7.3	5	50	plastic plate
exp_48	6.8-7.4	5	60	plastic plate
exp_43	1000	5	45	plastic plate
exp_44	1000	5	40	plastic plate
exp_45	1000	5	37	plastic plate

* Pressure range during the first two minutes of the experimental run

** Time period over which the mud was poured from the container

550

551 Table 1: Summary of measured and controlled variables for each experimental run.

552 **References**

553 Allen, C. C., Oehler, D., Etioppe, G., van Rensbergen, P., Baciuc, C., Feyzullayev, A., et al., 2013. Fluid
554 expulsion in terrestrial sedimentary basins: A process providing potential analogs for giant
555 polygons and mounds in the Martian lowlands. *Icarus*, 224(2), 424–432.
556 <https://doi.org/10.1016/j.icarus.2012.09.018>.

557 Bargery, A. S., Lane, S. J., Barrett, A., Wilson, L., Gilbert, J. S., 2010. The initial responses of hot liquid
558 water released under low atmospheric pressures: Experimental insights. *Icarus* 210(1), 488–506.
559 <https://doi.org/10.1016/j.icarus.2010.06.019>.

560 Brož, P., Hauber, E., 2013. Hydrovolcanic tuff rings and cones as indicators for phreatomagmatic
561 explosive eruptions on Mars. *Journal of Geophysical Research: Planets* 118, 1656–1675.
562 <https://doi.org/10.1002/jgre.20120>.

563 Brož, P., Čadež, O., Hauber, E., Rossi, A. P., 2014. Shape of scoria cones on Mars: Insights from
564 numerical modeling of ballistic pathways, *Earth and Planetary Science Letters* 406, 14–23,
565 <https://doi.org/10.1016/j.epsl.2014.09.002>.

566 Brož, P., Hauber, E., Wray, J. J., Michael, G., 2017. Amazonian volcanism inside Valles Marineris on
567 Mars. *Earth and Planetary Science Letters* 473, 122–130.
568 <https://doi.org/10.1016/j.epsl.2017.06.003>.

569 Brož, P., Hauber, E., van de Burgt, I., Špillar, V., Michael, G., 2019. Subsurface sediment mobilization
570 in the southern Chryse Planitia on Mars. *Journal of Geophysical Research: Planets* 124.
571 <https://doi.org/10.1029/2018JE005868>.

572 Brož, P., Krýza, O., Wilson, L., Conway, S. J., Hauber, E., Mazzini, A., Raack, J., Balme, M. R., Sylvest,
573 M. E., Patel, M. R. (in press). Experimental evidence for lava-like mud flows under Martian
574 surface conditions. *Nature Geoscience*.

575 Christensen, P.R., et al., 2001. Mars Global Surveyor Thermal Emission Spectrometer experiment:
576 Investigation description and surface science results. *Journal of Geophysical Research* 106,
577 23823–23872. <https://doi.org/10.1029/2000JE001370>.

578 Clark, B. C., 1978. Implications of abundant hygroscopic minerals in the martian regolith. *Icarus* 34,
579 645–665. [https://doi.org/10.1016/0019-1035\(78\)90052-0](https://doi.org/10.1016/0019-1035(78)90052-0).

580 Conway, S. J., Lamb, M. P., Balme, M. R., Towner, M. C., Murray, J. B., 2011. Enhanced runout and
581 erosion by overland flow at low pressure and subfreezing conditions: experiments and application
582 to Mars. *Icarus* 211, 443–457. <https://doi.org/10.1016/j.icarus.2010.08.026>.

583 Corradi, A. B., Manfredini T., Pellacani, G. C., Pozzi, P., 1994. Deflocculation of Concentrated Aqueous
584 Clay Suspensions with Sodium Polymethacrylates, *Journal of the American Ceramic Society* 77,
585 Issue 2. <https://doi.org/10.1111/j.1151-2916.1994.tb07022.x>.

586 Costard, F., Forget, F., Mangold, N., Peulvast, J. P., 2002. Formation of recent martian debris flows by
587 melting of near-surface ground ice at high obliquity. *Science* 295, 110–113.
588 <https://doi.org/10.1126/science.1066698>.

589 Forget, F., Hourdin, F., Fournier, R., Hourdin, C., Talagrand, O., Collins, M., Lewis, S. R., Read, P. L.,
590 Huot, J.-P., 1999. Improved general circulation models of the Martian atmosphere from the
591 surface to above 80 km. *Journal of Geophysical Research* 104, 24155.
592 <https://doi.org/10.1029/1999JE001025>.

593 Grott, M., Baratoux, D., Hauber, E., Sautter, V., Mustard, J., Gasnault, O., Ruff, S. W., Karato, S.-I.,
594 Debaille, V., Knapmeyer, M., Sohl, F., Van Hoolst, T., Breuer, D., Morschhauser, A., Toplis, M.
595 J., 2013. Long-Term Evolution of the Martian Crust-Mantle System, *Space Science Reviews* 174,
596 49–111. <https://doi.org/10.1007/s11214-012-9948-3>.

597 Hecht, M. H., 2002. Metastability of liquid water on Mars, *Icarus* 156, 373-386.
598 <https://doi.org/10.1006/icar.2001.6794>.

599 Hecht, M. H., et al., 2009. Detection of perchlorate and the soluble chemistry of martian soil at the
600 Phoenix lander site, *Science* 325, 64–67. <https://doi.org/10.1126/science.1172466>.

601 Herny, C., Conway, S.J., Raack, J., Carpy, S., Colleubanse, T., Patel, M.R., 2018. Downslope sediment
602 transport by boiling liquid water under Mars-like conditions: experiments and potential
603 implications for Martian gullies. In: Conway, S.J., Carrivick, J.L., Carling, P.A., De Haas, T.
604 Harrison, T.N. (eds) *Martian Gullies and their Earth Analogues*. Geological Society, London,
605 Special Publications 467. <https://doi.org/10.1144/SP467.10>.

606 Hemmi, R., Miyamoto, H., 2018. High resolution topographic analyses of mounds in southern Acidalia
607 Planitia, Mars: Implications for possible mud volcanism in submarine and subaerial
608 environments. *Geosciences* 8(5), 152. <https://doi.org/10.3390/geosciences8050152>.

609 Kiefer, H.H., Martin, T.Z., Peterfreund, A.R., Jakosky, B.M., Miner, E.D., Palluconi, F.D., 1977.
610 Thermal and albedo mapping of Mars during the Viking primary mission. *Journal of Geophysical*
611 *Research* 82, 4249–4291. <https://doi.org/10.1029/JS082i028p04249>.

612 Kilburn, C. R. J., 2000. Lava flows and flow fields, in *Encyclopedia of Volcanoes*, pp. 291 – 305,
613 Elsevier, New York.

614 Komatsu, G., Okubo, C. H., Wray, J. J., Ojha, L., Cardinale, M., Murana, A., Orosei, R., Chan, M. A.,
615 Ormö, J., Gallagher, R., 2016. Small edifice features in Chryse Planitia, Mars: assessment of a
616 mud volcano hypothesis, *Icarus* 268, 56–75. <http://dx.doi.org/10.1016/j.icarus.2015.12.032>.

617 Kopf, A. J., 2002. Significance of mud volcanism. *Review of Geophysics* 40, 1–52.
618 <https://doi.org/10.1029/2000RG000093>.

619 Kumar, P.S, Krishna, N., Prasanna Lakshmi, K.J., Raghukanth, S.T.G., Dhabu, A., Platz, T., 2019.
620 Recent seismicity in Valles Marineris, Mars: Insights from young faults, landslides, boulder falls

621 and possible mud volcanoes. *Earth and Planetary Science Letters* 505, 51–64.
622 <https://doi.org/10.1016/j.epsl.2018.10.008>.

623 Laskar J., Correia A. C. M., Gastineau M., Joutel F., Levrard B., Robutel P., 2004. Long term evolution
624 and chaotic diffusion of the insolation quantities of Mars. *Icarus* 170, 343–364.
625 <https://doi.org/10.1016/j.icarus.2004.04.005>.

626 Laigle, D., Coussot, P., 1997. Numerical modelling of mudflows. *Journal of Hydraulic Engineering* 123,
627 617–623. [https://doi.org/10.1061/\(ASCE\)0733-9429\(1997\)123:7\(617\)](https://doi.org/10.1061/(ASCE)0733-9429(1997)123:7(617)).

628 Massé, M., S. J. Conway, J. Gargani, M. R. Patel, K. Pasquon, A. McEwen, S. Carpy, V. Chevrier, M.
629 R. Balme, L. Ojha, et al., 2016. Transport processes induced by metastable boiling water under
630 Martian surface conditions, *Nature Geoscience* 9, 425–428. <http://doi.org/10.1038/ngeo2706>.

631 Mazzini, A., Etiopé, G., 2017. Mud volcanism: An updated review. *Earth-Science Reviews* 168, 81–
632 112. <https://doi.org/10.1016/j.earscirev.2017.03.001>

633 Miller, S. A., Mazzini, A., 2018. More than ten years of Lusi: A review of facts, coincidences, and past
634 and future studies. *Marine and Petroleum Geology* 90, 10–25.
635 <https://doi.org/10.1016/j.marpetgeo.2017.06.019>.

636 Montabone, L., Forget, F., Millour, E., Wilson, R. J., Lewis, S. R., Cantor, B., Kass, D., Kleinböhl, A.,
637 Lemmon, M. T., Smith, M. D., Wolff, M. J., 2015. Eight-year climatology of dust optical depth
638 on Mars. *Icarus* 251, 65. <https://doi.org/10.1016/j.icarus.2014.12.034>.

639 Morgan, P., Grott, M., Knapmeyer-Endrun, B., Golombek, M., Delage, P., Lognonné, P., Piqueux, S.,
640 Daubar, I., Murdoch, N., Charalambous, C., Pike, W. T., Müller, N., Hagermann, A., Siegler, M.,
641 Lichtenheldt, R., Teanby, N., Kedar, S., 2018. A Pre-Landing Assessment of Regolith Properties
642 at the InSight Landing Site. *Space Science Reviews* 214, 104. [https://doi.org/10.1007/s11214-](https://doi.org/10.1007/s11214-018-0537-y)
643 [018-0537-y](https://doi.org/10.1007/s11214-018-0537-y).

644 O'Brien, J. S., Julien, P. Y., 1988. Laboratory analysis of mudflow properties, *J. Hydraul. Eng.* 114,
645 877–887. [https://doi.org/10.1061/\(ASCE\)0733-9429\(1988\)114:8\(877\)](https://doi.org/10.1061/(ASCE)0733-9429(1988)114:8(877)).

646 Oehler, D. Z., Allen, C. C., 2012. Giant polygons and mounds in the lowlands of Mars: Signatures of an
647 Ancient Ocean? *Astrobiology* 12(6), 601–615. <https://doi.org/10.1089/ast.2011.0803>.

648 Oehler, D. Z., Etiope, G., 2017. Methane seepage on Mars: where to look and why, *Astrobiology* 17.
649 <https://doi.org/10.1089/ast.2017.1657>.

650 Okubo, C. H., 2016. Morphologic evidence of subsurface sediment mobilization and mud volcanism in
651 Candor and Coprates Chasmata, Valles Marineris, Mars, *Icarus* 269, 23–27.
652 <https://doi.org/10.1016/j.icarus.2015.12.051>.

653 Plesa, A.-C., Grott, M., Tosi, N., Breuer, D., Spohn, T., Wieczorek, M. A., 2016. How large are present-
654 day heat flux variations across the surface of Mars? *J. Geophys. Res. Planets* 121, 2386– 2403.
655 <https://doi.org/10.1002/2016JE005126>.

656 Pondrelli, M., Rossi, A. P., Ori, G. G., van Gasselt, S., Praeg, D., Ceramicola, S., 2011. Mud volcanoes
657 in the geologic record of Mars: The case of Firsoff crater. *Earth and Planetary Science Letters*
658 304(3-4), 511–519. <https://doi.org/10.1016/j.epsl.2011.02.027>.

659 Presley, M. A., Christensen, P. R., 1997. Thermal conductivity measurements of particulate materials 2.
660 Results. *Journal of Geophysical Research* 102, 6551–6566. <https://doi.org/10.1029/96JE03303>.

661 Putzig, N. E., Mellon, M. T., 2007. Apparent thermal inertia and the surface heterogeneity of Mars.
662 *Icarus* 191, 68–94. <https://doi.org/10.1016/j.icarus.2007.05.013>.

663 Raack, J., S. J. Conway, C. Herny, M. R. Balme, S. Carpy, Patel, M. R., 2017. Water-induced sediment
664 levitation enhances downslope transport on Mars, *Nature Communications* 8,
665 <https://doi.org/10.1038/s41467-017-01213-z>.

666 Ruesch, O., Genova A., Neumann W., Quick L. C., Castillo-Rogez J. C., Raymond C. A., Russel Ch.
667 T., Zuber, M. T., 2019. Slurry extrusion on Ceres from a convective mud-bearing mantle. *Nature*
668 *Geoscience* 12, 505–509. <https://doi.org/10.1038/s41561-019-0378-7>.

669 Rubin, D.M, Fairen, A., Martínez-Frías, J., Frydenvang, J., Gasnault, O., Galfenbaum, G., Goetz, W.,
670 Grotzinger, J.P., Le Moué'lic, S., Mangold, N., Newsom, H., Oehler, D.Z., Rapin, W., Schieber,

671 J., Weins, R.C., 2017. Fluidized-sediment pipes in Gale Crater, Mars, and possible Earth analogs.
672 *Geology* 45, 7–10. <https://doi.org/10.1130/G38339.1>.

673 Salvatore, M. R., Christensen, P. R., 2015. On the origin of the Vastitas Borealis formation in Chryse
674 and Acidalia Planitiae, Mars. *Journal of Geophysical Research: Planets* 119, 2437–2456.
675 <https://doi.org/10.1002/2014JE004682>.

676 Sinton, W., Strong, J., 1960. Radiometric observations of Mars, *Astrophysical Journal* 131, 459–469.
677 <https://doi.org/10.1086/146852>.

678 Skinner, J. A., Tanaka, K. L., 2007. Evidence for and implications of sedimentary diapirism and mud
679 volcanism in the southern Utopia highland-lowland boundary plain, Mars, *Icarus* 186, 41–59,
680 <http://dx.doi.org/10.1016/j.icarus.2006.08.013>.

681 Skinner, J. A., Mazzini, A., 2009. Martian mud volcanism: Terrestrial analogs and implications for
682 formational scenarios. *Marine and Petroleum Geology* 26(9), 1866–1878.
683 <https://doi.org/10.1016/j.marpetgeo.2009.02.006>.

684 Vaniman, D. T., Bish, D. L., Chipewa, S. J., Fialips, C. I., Carrey, J. W. Feldman, W. C., 2004.
685 Magnesium sulphate salts and the history of water on Mars. *Nature* 431, 663– 665.
686 <https://doi.org/10.1038/nature02973>.

687 Ward, W. R., 1973. Large-scale variations in the obliquity of Mars. *Science* 181, 260–262.
688 <https://doi.org/10.1126/science.181.4096.260>.

689 Whaetley, D. F., Chan, M. A., Okubo, C. H., 2019. Clastic pipes and mud volcanism across Mars:
690 Terrestrial analog evidence of past martian groundwater and subsurface fluid mobilization. *Icarus*
691 328, 141-151. <https://doi.org/10.1016/j.icarus.2019.02.002>.

692 Wilson, L., Head, J.W., 1994. Mars: review and analysis of volcanic eruption theory and relationships
693 to observed landforms. *Rev. Geophys.* 32, 221–263. <https://doi.org/10.1029/94RG01113>.

694 Wilson, L., and Mouginis-Mark, P. J., 2014. Dynamics of a fluid flow on Mars: Lava or mud? *Icarus*
695 233, 268–280. <https://doi.org/10.1016/j.icarus.2014.01.041>.